JOURNAL OF GUIDANCE, CONTROL, AND DYNAMICS
Vol. 30, No. 5, September–October 2007

High-Order Quasi-Linearization Technique for Identification of Linear-Fractional-Transformation-Modeled Aeroservoelastic Systems

Boris Moulin*
Technion—Israel Institute of Technology, 32000 Haifa, Israel

DOI: 10.2514/1.27652

High-order quasi-linearization procedures were developed for identification of nonlinear dynamic systems modeled by a parameter-dependent linear-fractional transformation containing a linear dynamic system in the feedforward pass and a static nonlinear element in the feedback loop. The developed procedures enable estimation of unknown parameters of both linear and nonlinear components of the model. The proposed approach for synthesis of the high-order quasi-linearization procedures enables construction of a variety of estimation algorithms. Two third-order-of-convergence estimation algorithms are constructed and compared with the second-order-of-convergence classical Bellman–Kalaba quasi-linearization procedure. A numerical application for an unmanned aerial vehicle is used to demonstrate the developed technique. Parameters of the vehicle linear aeroservoelastic model and of the nonlinear damping are estimated. Simulation results demonstrate that the range and rate of convergence of the suggested third-order methods are greater than those of the second-order quasi-linearization technique.

Nomenclature

A, $B_{(\cdot)}$, $C_{(\cdot)}$, $D_{(\cdot)}$	=	state-space matrices
$A_{h0,1,2}$, D_h, E	=	rational aerodynamic approximation matrices
a_{ij}	=	parameters of interpolation function
$f(\cdot,\cdot)$	=	nonlinear function of the feedback element
I	=	identity matrix
J	=	performance index
$M^{(\cdot)}_{(\cdot)}$, $H^{(\cdot)}_{(\cdot)}$, $G^{(\cdot)}_{(\cdot)}$, $L^{(\cdot)}_{(\cdot)}$, $N^{(\cdot)}_{(\cdot)}$, $\eta^{(\cdot)}_{(\cdot)}$	=	matrix coefficients of the linearized linear-fractional-transformation model
$\bar{M}^{(\cdot)}_{(\cdot)}$, $\bar{H}^{(\cdot)}_{(\cdot)}$, $\bar{\eta}^{(\cdot)}_{(\cdot)}$	=	matrix coefficients of the linearized state-space model
M_{hc}	=	mass coupling matrix between control and structural modes
M_{hh}, B_{hh}, K_{hh}	=	generalized mass, damping, and stiffness matrices
p, q	=	input and output vectors of the nonlinear element
q_∞	=	dynamic pressure
R	=	aerodynamic lag matrix
r	=	order of convergence
V	=	true airspeed
x, u, y, v	=	state, input, output, and measurement noise vectors
Y_z	=	sensitivity function of measurements to initial conditions and parameters
z	=	extended state vector
α, β, θ	=	vectors of unknown parameters
γ_{ij}	=	parameters of interpolation function
δ_c	=	control-surface commanded deflections
λ	=	particular solution of the linearized system
ξ	=	vector of generalized displacements
ϕ_{nh}, ϕ_{nc}	=	normal and control modes for the nonlinearity degrees of freedom
ϕ_{yh}, ϕ_{yc}	=	normal and control modes for the output degrees of freedom
Ω	=	fundamental matrix of the linearized system

Presented as Paper 2034 at the AIAA/ASME/ASCE/AHS/ASC 47th Structures, Structural Dynamics and Materials Conference, Newport, RI, 1–4 May 2006; received 5 September 2006; revision received 15 April 2007; accepted for publication 30 April 2007.

*Senior Researcher, Faculty of Aerospace Engineering. Member AIAA.

I. Introduction

SYSTEM identification plays a considerable role in aerospace design as an important tool in flight vehicle modeling, control, and data analysis [1]. A retrospective on the development of modern parameter identification methods and software presented in [2] demonstrates continuous interest in this problem.

This paper presents a quasi-linearization-based approach for parameter estimation of the systems described by a state-space linear-fractional-transformation (LFT) model containing a linear time-invariant system in its feedforward pass and a static nonlinear element in the feedback loop. An LFT approach to parameter estimation has been provided in [3]. The parameters to be estimated appear in this approach as a separate feedback block of the LFT accomplished by known static nonlinear and time-varying linear feedback elements. The parameter estimation is performed using a gradient-based optimization technique. Identification of unknown dynamics of aeroelastic systems using the LFT framework was suggested in [4]. Feedback-interconnected models were used in [5] for block-oriented identification of static nonlinearities in nonlinear aeroelastic systems.

The quasi-linearization technique applied in this study was developed by Bellman and Kalaba [6]. It presents a general approach for solution of various problems of mathematics and control (e.g., solution of ordinary and partial differential equations with initial and boundary conditions) [6–8]. The basic principle of quasi linearization is representation of a nonlinear problem as a sequence of linear problems. This leads to the iterative technique based on the solution of the constructed sequence of the linear problems approximating the original nonlinear one. When the conditions of convergence are fulfilled, the sequence of the solutions of the linear problems is converged to the solution of the nonlinear problem. The quasi linearization may be considered as a generalization of the Newton–Raphson technique to solve problems in a functional space [7]. On the other hand, it may be considered as a realization of the abstract Newton–Raphson method (or Newton–Raphson–Kantorovich method), in which the problem is solved in the Banach space of all continuous differentiable functions satisfying prescribed

boundary conditions [8]. To expand the region and increase the rate of convergence of the quasi-linearization algorithms, high-order methods for solution of functional equations can be employed for synthesis of the quasi-linearization procedures. Quasi-linearization algorithms based on the third-order-of-convergence methods of tangent parabolas [9,10] and hyperbolas [10,11] were suggested in [8] for solution of two-point boundary value problems. A class of high-order quasi-linearization algorithms for solution of the identification problem was developed in [12]. The synthesis of these algorithms is based on a proposed technique enabling construction of the quasi-linearization procedures of the required order of convergence. This technique enables constraining of the highest order of the derivatives of the model nonlinearities with respect to the states and estimating parameters to be used in the iterative procedure. As indicated in the detailed survey of Hamel and Jategaonkar [13] the quasi-linearization technique is applied in aerospace industries for aircraft parameter estimation (see [14–16]).

This study presents the high-order quasi-linearization technique for identification of the LFT-modeled dynamic systems, particularly, aeroelastic/aeroservoelastic (ASE) systems. In Sec. II of the paper, a brief description of the quasi-linearization technique for identification of the systems described by standard state-space models is presented. The LFT-modeled systems are considered in Sec. III. This study focuses on parameter estimation of the LFT interconnection containing unknown parameters in both linear and nonlinear components of the model. Sections IV and V present the second- and high-order techniques for identification of the LFT-modeled systems. The numerical example in Sec. VI demonstrates the application of the developed identification procedures for parameter estimation of the ASE model of a generic unmanned aerial vehicle (UAV). The ASE model of the UAV contains actuator nonlinear damping for which the parameter is estimated together with the parameters of the linear dynamic system. Results of comparison of the convergence range and rate of the suggested quasi-linearization algorithms are presented.

II. Quasi-Linearization Technique for System Identification

Consider a problem of identification for a nonlinear state-space model:

$$\dot{x} = \tilde{\Psi}(x, \alpha, u, t), \qquad x(t_0) = x_0 \tag{1}$$

$$y = \tilde{h}(x, \alpha, u, t) + v(t) \tag{2}$$

where α is the vector of unknown time-invariant parameters, v is the vector of measurement noise, and $\tilde{\Psi}(\cdot)$ and $\tilde{h}(\cdot)$ are the nonlinear vector functions.

The model of Eqs. (1) and (2) can be written in extended state space to obtain a compact formulation of the identification problem [7]:

$$\dot{z} = \Psi(z, u, t), \qquad z(t_0) = z_0 \tag{3}$$

$$y = h(z, u, t) + v(t) \tag{4}$$

where $z = [x^T \ \ \alpha^T]^T$ is the extended state vector, and the vector function $\Psi(\cdot)$ is defined as

$$\Psi(z, u, t) = [\,\tilde{\Psi}^T(x, \alpha, u, t) \quad 0\,]^T$$

The problem of identification is to obtain the estimates of the vector of initial conditions x_0 and parameters α using the measurements of the system input $u(t)$ and output $y(t)$. The estimates must minimize the certain performance index, which is usually defined as

$$J = \sum_{i=1}^{N} [y(t_i) - y^M(t_i)]^T Q(t_i) [y(t_i) - y^M(t_i)] \tag{5}$$

where $y^M(t)$ is the vector of the model outputs, $Q(t)$ is the positive-definite symmetric weighting matrix, and N is the number of discrete measurements of the vector y.

The quasi-linearization technique is based on the representation of a nonlinear problem as a sequence of linear problems. The classic Bellman–Kalaba algorithm applies linearization based on the first-order Taylor series expansion of the nonlinear model about the kth approximation of the vectors of states and parameters to be estimated. The resulting linearized model is expressed as

$$\dot{x}_{k+1} = \tilde{\Psi}_k + \frac{\partial \tilde{\Psi}_k}{\partial x_k}(x_{k+1} - x_k) + \frac{\partial \tilde{\Psi}_k}{\partial \alpha_k}(\alpha_{k+1} - \alpha_k) \qquad x_{k+1}(t_0) = x_{0,k+1} \tag{6}$$

$$y_{k+1} = \tilde{h}_k + \frac{\partial \tilde{h}_k}{\partial x_k}(x_{k+1} - x_k) + \frac{\partial \tilde{h}_k}{\partial \alpha_k}(\alpha_{k+1} - \alpha_k) \tag{7}$$

where x_{k+1} and $x_{0,k+1}$ are the $k+1$ approximations of the vectors x and x_0, and where

$$\tilde{\Psi}_k = \tilde{\Psi}(x_k, \alpha_k, u, t), \qquad \tilde{h}_k = \tilde{h}(x_k, \alpha_k, u, t)$$

This linearization leads to a sequence of linear least-squares problems. When the conditions of convergence are fulfilled, the sequence of the solutions of the linear problems is converged to the solution of the nonlinear problem. Sufficient conditions for convergence of the quasi-linearization iterative process are provided in [6]. These conditions can be applied for the identification problem of Eqs. (1) and (2) if the measurement function $\tilde{h}(\cdot)$ is linear with respect to x and the measurement noise can be ignored [i.e., $y(t) = Cx(t)$]. Then the quasi-linearization process is converged quadratically if the function $\tilde{\Psi}(x, \alpha, u, t)$ is convex and if the off-diagonal elements of the matrix function $\partial\tilde{\Psi}/\partial x$ are positive [17]. These requirements are rather strict and provide conservative evaluation of the convergence range.

III. Nonlinear LFT Model of an Aeroservoelastic System

The nonlinear LFT model under consideration is represented by the following equations:

$$\dot{x} = A(\theta)x + B_1(\theta)u + B_2(\theta)q, \qquad x(t_0) = x_0 \tag{8}$$

$$y = C_1(\theta)x + D_{11}(\theta)u + D_{12}(\theta)q + v \tag{9}$$

$$p = C_2(\theta)x + D_{21}(\theta)u + D_{22}(\theta)q \tag{10}$$

$$q = f(p, \beta) \tag{11}$$

where x, u, and y are the vectors of states, inputs, and outputs of the system, as shown in Fig. 1; p and q are the vectors of inputs and outputs of the nonlinear static element defined by the nonlinear function $f(\cdot)$; and θ and β are the vectors of unknown parameters of the linear system and nonlinear element.

The linear time-invariant system forming the feedforward pass of the model is described by the matrices A, B_j, C_i, and D_{ij} of

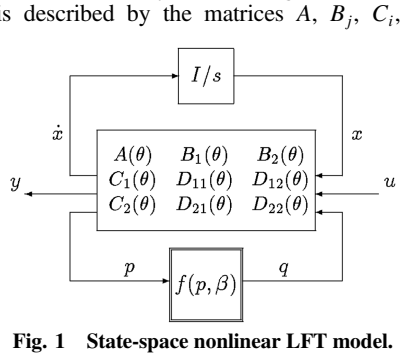

Fig. 1 State-space nonlinear LFT model.

Eqs. (8–10). The matrices A, B_1, C_1, and D_{11} define the nominal linear system. The matrices B_2, C_2, D_{12}, D_{21}, and D_{22} define additional inputs and outputs for interconnection of the linear system with the nonlinear element of Eq. (11). For the ASE systems, the term $B_2 q$ of Eq. (8) defines the generalized forces introduced to the system by nonlinearity $f(\cdot)$. The terms $D_{12}q$ and $D_{22}q$ are the components added to the system outputs by this nonlinearity. The matrices C_2 and D_{21} are required for construction of the output p, which is not a physical output of the system, but a variable required for generation of the forces q introduced by the nonlinear element (for example, if q represents nonlinear damping forces, then p is the structural velocity).

State-space ASE modeling is based on the rational approximation of the unsteady generalized aerodynamic force matrices in the Laplace domain, of the form [18,19]

$$\tilde{Q}_h(s) = A_{h0} + \frac{b}{V}A_{h1}s + \frac{b^2}{V^2}A_{h2}s^2 + D_h\left(Is - \frac{V}{b}R\right)^{-1}Es \quad (12)$$

where R is the aerodynamic lag matrix and A_{hi}, D_h, and E are the rational aerodynamic approximation matrices that are determined in a nonlinear least-squares solution [19]. The A_{hi} and E approximation matrices are column-partitioned according to the structural, control, and gust modes as

$$A_{h_i} = [\,A_{hh_i} \quad A_{hc_i} \quad A_{hG_i}\,] \qquad (i = 0, 1, 2)$$

and

$$E = [\,E_h \quad E_c \quad E_G\,]$$

For the ASE plant with actuator inputs u and sensor outputs y, the state vector x includes generalized structural displacements ξ and velocities $\dot{\xi}$; aerodynamic states x_a; and actuator states δ_c, $\dot{\delta}_c$, and $\ddot{\delta}_c$ (representing control-surface commanded deflections, velocities, and accelerations); leading to the state vector

$$x = \left[\xi^T \;\; \dot{\xi}^T \;\; x_a^T \;\; \delta_c^T \;\; \dot{\delta}_c^T \;\; \ddot{\delta}_c^T\right]^T$$

The matrices A, B_1, and D_{11} of Eqs. (8) and (9) are constructed according to [18] as

$$[A] = \begin{bmatrix} A_{ae} & B_{ae} \\ 0 & A_{ac} \end{bmatrix}, \qquad [B_1] = \begin{bmatrix} 0 \\ B_{ac} \end{bmatrix}, \qquad [D_{11}] = 0 \quad (13)$$

with

$$A_{ae} = \begin{bmatrix} 0 & I & 0 \\ -\bar{M}_{hh}^{-1}\bar{K}_{hh} & -\bar{M}_{hh}^{-1}\bar{B}_{hh} & -q\bar{M}_{hh}^{-1}D_h \\ 0 & E_h & \frac{V}{b}R \end{bmatrix}$$

$$B_{ae} = \begin{bmatrix} 0 & 0 & 0 \\ -\bar{M}_{hh}^{-1}\bar{K}_{hc} & -\bar{M}_{hh}^{-1}\bar{B}_{hc} & -\bar{M}_{hh}^{-1}\bar{M}_{hc} \\ 0 & E_c & 0 \end{bmatrix}$$

where

$$\bar{M}_{hh} = M_{hh} + \frac{q_\infty b^2}{V^2}A_{hh_2}, \qquad \bar{K}_{hh} = K_{hh} + q_\infty A_{hh_0}$$

$$\bar{B}_{hh} = B_{hh} + \frac{q_\infty b}{V}A_{hh_1} \qquad \bar{K}_{hc} = q_\infty A_{hc_0}, \qquad \bar{B}_{hc} = \frac{q_\infty b}{V}A_{hc_1}$$

$$\bar{M}_{hc} = M_{hc} + \frac{q_\infty b^2}{V^2}A_{hc_2}$$

and the matrices A_{ac} and B_{ac} are obtained from the state-space representation of the control-surface actuators.

In the current study, definition of the matrices C_i of Eqs. (9) and (10) is generalized to include control-surface commanded deflections, velocities, and accelerations. A control-surface deflection is expressed as a superposition of the structural displacements due to elastic deformations of the structure and the displacements induced by control command. The deflection of a structural or aerodynamic degree of freedom is expressed as

$$y_1 = \phi_{yh}\xi + \phi_{yc}\delta_c \quad (14)$$

where ϕ_{yh} and ϕ_{yc} are the matrices of the normal and control modes for the degrees of freedom prescribed for the output. A control mode is defined by the displacement vector of the undeformed aircraft, with a unit deflection of one control surface [20]. Therefore, the second term of Eq. (14), representing a control-surface commanded deflection, is zero for the rest of the aircraft structure, except the control surface. According to Eq. (14) and the component representation of the state vector shown earlier, the matrix C for displacement measurements is presented as

$$C_i = [\,\phi_{yh} \quad 0 \quad 0 \quad \phi_{yc} \quad 0 \quad 0\,] \quad (15)$$

The velocities and acceleration measurements are obtained with

$$C_i = [\,0 \quad \phi_{yh} \quad 0 \quad 0 \quad \phi_{yc} \quad 0\,] \quad (16)$$

and

$$C_i = \phi_{yh}A^{(2)} + [\,0 \quad 0 \quad 0 \quad 0 \quad 0 \quad \phi_{yc}\,] \quad (17)$$

where $A^{(2)}$ is the second block row of the matrix A, corresponding to the $\ddot{\xi}$ component of the vector $\dot{x}$.

Construction of the matrices B_2, C_2, D_{12}, D_{21}, and D_{22} is shown in detail in [21]. For example, these matrices constructed for modeling of the local nonlinear damping are expressed as

$$B_2 = \begin{bmatrix} 0 \\ -\bar{M}_{hh}^{-1}\phi_{nh}^T \end{bmatrix}, \qquad C_2 = [\,0 \quad \phi_{nh} \quad 0 \quad 0 \quad \phi_{nc} \quad 0\,] \qquad D_{ij} = 0 \quad (18)$$

where ϕ_{nh} and ϕ_{nc} are the normal and control modes for the degrees of freedom involved in the nonlinearity modeling.

The model of the closed-loop system is obtained by augmentation of the presented ASE plant model with the control-system state-space model, as shown in [21].

The LFT model of Eqs. (8–11) is an *adequate* representation of aerostructural systems, with internal structural and aerodynamic forces being presented as a function of displacements, velocities, and accelerations of the structure [21]. Control-system nonlinearities are presented in the LFT framework as well. The LFT model enables use of a priori knowledge about the ASE system to be identified. Usually, an initial linear model of the ASE system is built before the identification process, using structural and aerodynamic models of an aircraft. Another advantage of the LFT interconnection is its flexibility. It enables modeling of local nonlinearities of the system (nonlinear control-surface actuators, external store attachments or aerodynamics, hinge friction, etc.) as well as global nonlinearities. The local nonlinearities are described by the variables p and q, representing physical degrees of freedom of the structure (displacements, forces, etc.), and the global nonlinearities are presented by the modal coordinate p and q. Different nonlinearities can be applied without or with minor altering of the linear model, because the matrices A, B_1, C_1, and D_{11} are invariant to nonlinearity. The LFT model is general; for example, the Hammerstein, Wiener, and feedback models are particular cases of the LFT interconnection [5].

IV. Quasi-Linearization Technique for Identification of LFT-Modeled Systems

The problem of identification of an LFT-modeled system defined by the model of Eqs. (8–11) is to obtain the estimates of the vector of initial conditions x_0 and the vectors of unknown parameters θ and β, minimizing the performance index of Eq. (5).

According to the quasi-linearization technique, the model of Eqs. (8–11) should be linearized to be presented in the form

$$\dot{x}_{k+1,j} = \bar{M}_x^{k,j}x_{k+1,j} + \bar{M}_\theta^{k,j}\theta_{k+1,j} + \bar{M}_\beta^{k,j}\beta_{k+1,j} + \bar{\eta}_x^{k,j} \qquad x_{k+1,j}(t_0) = x_{0,k+1,j} \quad (19)$$

$$y_{k+1,j} = \bar{H}_x^{k,j} x_{k+1,j} + \bar{H}_\theta^{k,j} \theta_{k+1,j} + \bar{H}_\beta^{k,j} \beta_{k+1,j} + \bar{\eta}_y^{k,j} \tag{20}$$

where $x_{k+1,j}$, $\theta_{k+1,j}$, and $\beta_{k+1,j}$ are the approximations of the vectors x, θ, and β; and $\bar{M}_{(\cdot)}^{k,j}$, $\bar{H}_{(\cdot)}^{k,j}$, and $\bar{\eta}_{(\cdot)}^{k,j}$ are the coefficient matrices depending on the kth approximations of x, θ, and β. Although the square matrices $\bar{M}_{(\cdot)}^{k,j}$ and $\bar{H}_{(\cdot)}^{k,j}$ represent the homogeneous part of the model, the vectors $\bar{\eta}_{(\cdot)}^{k,j}$ accumulate all nonhomogeneous terms of the initial model of Eqs. (8–11) and the nonhomogeneous terms obtained in the linearization process (see Appendices A and B).

For the sake of consistency with the high-order algorithms to be considered, the sub- and superscript j is presented in the preceding equations. For the classic quasi-linearization technique, j is set to 1 and does not vary in the iteration process.

Construction of the linearized model of Eqs. (19) and (20) starts with substitution of Eq. (11) into Eqs. (8–10):

$$\dot{x} = A(\theta)x + B_1(\theta)u + B_2(\theta)f(p,\beta), \qquad x(t_0) = x_0 \tag{21}$$

$$y = C_1(\theta)x + D_{11}(\theta)u + D_{12}(\theta)f(p,\beta) \tag{22}$$

$$p = C_2(\theta)x + D_{21}(\theta)u + D_{22}(\theta)f(p,\beta) \tag{23}$$

Performing the Taylor expansion about the kth approximation of x, p, θ, and β obtains the linear model with a linear feedback:

$$\begin{aligned}\dot{x}_{k+1,j} = {} & M_x^{k,j} x_{k+1,j} + M_\theta^{k,j} \theta_{k+1,j} + L_x^{k,j} N_p^{k,j} p_{k+1,j} \\ & + L_x^{k,j} N_\beta^{k,j} \beta_{k+1,j} + \eta_x^{k,j}\end{aligned} \tag{24}$$

$$\begin{aligned}y_{k+1,j} = {} & H_x^{k,j} x_{k+1,j} + H_\theta^{k,j} \theta_{k+1,j} + L_y^{k,j} N_p^{k,j} p_{k+1,j} \\ & + L_y^{k,j} N_\beta^{k,j} \beta_{k+1,j} + \eta_y^{k,j}\end{aligned} \tag{25}$$

$$\begin{aligned}p_{k+1,j} = {} & G_x^{k,j} x_{k+1,j} + G_\theta^{k,j} \theta_{k+1,j} + L_p^{k,j} N_p^{k,j} p_{k+1,j} \\ & + L_p^{k,j} N_\beta^{k,j} \beta_{k+1,j} + \eta_p^{k,j}\end{aligned} \tag{26}$$

The matrix coefficients of Eqs. (24–26) for $j = 1$ are presented in Appendix A.

By performing LFT operations, the model of Eqs. (24–26) is transformed to the required model of Eqs. (19) and (20) with the matrix coefficients provided in Appendix B. The resulting model of Eqs. (19) and (20) can be written in extended state space to obtain a compact formulation of identification algorithms. Define the extended vector of the states as

$$z_{k+1,j} = \begin{bmatrix} x_{k+1,j}^T & \theta_{k+1,j}^T & \beta_{k+1,j}^T \end{bmatrix}^T$$

Then the linearized model in extended state space becomes

$$\dot{z}_{k+1,j} = \bar{M}^{k,j} z_{k+1,j} + \bar{\eta}^{k,j}, \qquad z_{k+1,j}(t_0) = z_{0,k+1,j} \tag{27}$$

$$y_{k+1,j} = \bar{H}^k z_{k+1,j} + \bar{\eta}_y^{k,j} \tag{28}$$

where

$$\bar{M}^{k,j} = \begin{bmatrix} \bar{M}_x^{k,j} & \bar{M}_\theta^{k,j} & \bar{M}_\beta^{k,j} \\ 0 & 0 & 0 \\ 0 & 0 & 0 \end{bmatrix}, \qquad \bar{H}^{k,j} = \begin{bmatrix} \bar{H}_x^{k,j} & \bar{H}_\theta^{k,j} & \bar{H}_\beta^{k,j} \end{bmatrix}$$

$$\bar{\eta}^{k,j} = \begin{bmatrix} \bar{\eta}_x^{k,j} \\ 0 \\ 0 \end{bmatrix}$$

According to the quasi-linearization technique, the solution of Eq. (27) is defined as

$$z_{k+1,j}(t) = \Omega_{k+1,j}(t_0,t) z_{0,k+1,j} + \lambda_{k+1,j}(t) \tag{29}$$

where $\Omega_{k+1,j}(t_0,t)$ and $\lambda_{k+1,j}(t)$ are the fundamental matrix and the particular solution of Eq. (27).

Equation (29) represents the estimate $z_{k+1,j}(t)$ of the extended state vector z as a function of the estimate $z_{0,k+1,j}$ of the initial conditions z_0. Substituting Eqs. (28) and (29) into the performance index of Eq. (5) obtains the linear least-squares problem for the estimate of the vector $z_{0,k+1,j}$. Minimizing the performance index $J(z_{0,k+1,j})$ with respect to $z_{0,k+1,j}$ obtains

$$\begin{aligned}z_{0,k+1,j} = V_{k+1,j}^{-1} \Bigg\{ & \sum_{i=1}^{N} \Omega_{k+1,j}(t_0,t_i)^T \bar{H}^{k,j}(t_i)^T Q(t_i) [y(t_i) - \bar{\eta}_y^{k,j}(t_i) \\ & - \bar{H}^{k,j}(t_i) \lambda_{k+1,j}(t_i)] \Bigg\}\end{aligned} \tag{30}$$

where

$$V_{k+1,j} = \sum_{i=1}^{N} \Omega_{k+1,j}(t_0,t_i)^T \bar{H}^{k,j}(t_i)^T Q(t_i) \bar{H}^{k,j}(t_i) \Omega_{k+1,j}(t_0,t_i)$$

Substituting the approximation $z_{0,k+1}$ into the expression (29) obtains the estimate $z_{k+1}(t)$ of the extended state vector z.

The presented quasi-linearization algorithm based on the first-order Taylor series expansion guarantees the second order of convergence in the convergence range.

V. High-Order Quasi-Linearization Technique

The high-order quasi-linearization technique was suggested in [12] to expand the region and increase the rate of convergence of the second-order procedure. The most general formulation of the high-order technique is based on the interpolation function suggested in [22] for solution of algebraic and transcendental equations. For the nonlinear model of Eq. (3), this interpolation function is set as

$$\hat{\Psi}(z_{k+1},u,t) = \sum_{j=0}^{l} \frac{1}{j!} \sum_{i=1}^{r_j} a_{ij} \Psi^{(j)} \Big|_{z=z_k+\gamma_{ij}(z_{k+1}-z_k)} (z_{k+1} - z_k)^j \tag{31}$$

where $\Psi^{(j)}(\cdot)$ is the jth derivative of $\Psi(\cdot)$ with respect to z.

The parameters a_{ij}, γ_{ij} are chosen to satisfy the conditions

$$\hat{\Psi}^{(j)}(z_k,u,t) = \Psi^{(j)}(z_k,u,t), \qquad j = \overline{0,(r-1)} \tag{32}$$

where r is the required order of convergence of the iterative procedure.

The first-order Taylor approximation applied in the classic quasi-linearization procedure can be obtained from Eq. (31) by setting $l = 1$, $r_j = 1$, $a_{ij} = 1$, and $\gamma_{ij} = 0$. This approximation satisfies the requirements of Eq. (32) for $j = 0, 1$.

Two quasi-linearization algorithms of the third order of convergence will be constructed for identification of the LFT-modeled systems. These algorithms are chosen from a variety of methods provided by the interpolation function of Eq. (31), because their convergence is proved for solution of functional equations.

A. Quasi Linearization Based on the Method of Tangent Hyperbolas

The method of tangent hyperbolas for solution of functional equations was suggested in [11]. It guarantees the third order of convergence, and so the error in the $k+1$ iteration is proportional to the cube of the error in the kth iteration [11]. This method is based on the Taylor series expansion keeping the terms up to the second order. It can be also obtained from the function of Eq. (31) by setting $l = 2$, $r_j = 1$, $a_{ij} = 1$, and $\gamma_{ij} = 0$.

The high-order quasi-linearization procedures employ a multistep iteration scheme in which the accuracy of approximation is increased step by step within each iteration. The number of steps is equal to the method order of convergence minus one. For the model of Eq. (3), the

method of tangent hyperbolas leads to a two-step iteration with the linearized equations in the form

$$\dot{z}_{k+1,1} = \Psi_k + \frac{\partial \Psi_k}{\partial z_k}(z_{k+1,1} - z_k)$$
$$\dot{z}_{k+1,2} = \Psi_k + \frac{\partial \Psi_k}{\partial z_k}(z_{k+1,2} - z_k) + \frac{1}{2}\frac{\partial^2 \Psi_k}{\partial z_k^2}(z_{k+1,1} - z_k)(z_{k+1,2} - z_k) \tag{33}$$

It should be noticed that the first step of the high-order procedure represents an iteration of the second-order algorithm. For the LFT model of Eqs. (8–11), the first-step linearized model of Eqs. (19) and (20) is defined by the matrix coefficients of Eqs. (A1–A7). The first step results with the approximations $x_{k+1,1}$, $\theta_{k+1,1}$, and $\beta_{k+1,1}$. According to the method of tangent hyperbolas, the second step of the iteration is based on the following approximation of Eq. (22) [Eqs. (22) and (23) are similarly linearized]:

$$\begin{aligned}
\dot{x}_{k+1,2} &= A(\theta_k)x_k + B_1(\theta_k)u + B_2(\theta_k)f(p_k,\beta_k) \\
&+ A(\theta_k)(x_{k+1,2} - x_k) + \frac{\partial A(\theta_k)}{\partial \theta_k}x_k(\theta_{k+1,2} - \theta_k) \\
&+ \frac{\partial B_1(\theta_k)}{\partial \theta_k}u(\theta_{k+1,2} - \theta_k) + \frac{\partial B_2(\theta_k)}{\partial \theta_k}f(p_k,\beta_k)(\theta_{k+1,2} - \theta_k) \\
&+ B_2(\theta_k)\frac{\partial f_k}{\partial p_k}(p_{k+1,2} - p_k) + B_2(\theta_k)\frac{\partial f_k}{\partial \beta_k}(\beta_{k+1,2} - \beta_k) \\
&+ \frac{1}{2}\frac{\partial A(\theta_k)}{\partial \theta_k}(\theta_{k+1,1} - \theta_k)(x_{k+1,2} - x_k) \\
&+ \frac{1}{2}\frac{\partial A(\theta_k)}{\partial \theta_k}(x_{k+1,1} - x_k)(\theta_{k+1,2} - \theta_k) \\
&+ \frac{1}{2}\frac{\partial^2 A(\theta_k)}{\partial \theta_k^2}x_k(\theta_{k+1,1} - \theta_k)(\theta_{k+1,2} - \theta_k) \\
&+ \frac{1}{2}\frac{\partial^2 B_1(\theta_k)}{\partial \theta_k^2}u(\theta_{k+1,1} - \theta_k)(\theta_{k+1,2} - \theta_k) \\
&+ \frac{1}{2}\frac{\partial^2 B_2(\theta_k)}{\partial \theta_k^2}f(p_k,\beta_k)(\theta_{k+1,1} - \theta_k)(\theta_{k+1,2} - \theta_k) \\
&+ \frac{1}{2}\frac{\partial B_2(\theta_k)}{\partial \theta_k}\frac{\partial f_k}{\partial p_k}(p_{k+1,1} - p_k)(\theta_{k+1,2} - \theta_k) \\
&+ \frac{1}{2}\frac{\partial B_2(\theta_k)}{\partial \theta_k}\frac{\partial f_k}{\partial \beta_k}(\beta_{k+1,1} - \beta_k)(\theta_{k+1,2} - \theta_k) \\
&+ \frac{1}{2}\frac{\partial B_2(\theta_k)}{\partial \theta_k}(\theta_{k+1,1} - \theta_k)\frac{\partial f_k}{\partial p_k}(p_{k+1,2} - p_k) \\
&+ \frac{1}{2}\frac{\partial B_2(\theta_k)}{\partial \theta_k}(\theta_{k+1,1} - \theta_k)\frac{\partial f_k}{\partial \beta_k}(\beta_{k+1,2} - \beta_k) \\
&+ \frac{1}{2}B_2(\theta_k)\frac{\partial^2 f_k}{\partial p_k^2}(p_{k+1,1} - p_k)(p_{k+1,2} - p_k) \\
&+ \frac{1}{2}B_2(\theta_k)\frac{\partial^2 f_k}{\partial \beta_k \partial p_k}(\beta_{k+1,1} - \beta_k)(p_{k+1,2} - p_k) \\
&+ \frac{1}{2}B_2(\theta_k)\frac{\partial^2 f_k}{\partial p_k \partial \beta_k}(p_{k+1,1} - p_k)(\beta_{k+1,2} - \beta_k) \\
&+ \frac{1}{2}B_2(\theta_k)\frac{\partial^2 f_k}{\partial \beta_k^2}(\beta_{k+1,1} - \beta_k)(\beta_{k+1,2} - \beta_k)
\end{aligned} \tag{34}$$

The second-step matrix coefficients of Eq. (24) are defined as follows [the coefficients of Eqs. (25) and (26) are similarly derived]:

$$M_x^{k,2} = A(\theta_k) + \frac{1}{2}\frac{\partial A(\theta_k)}{\partial \theta_k}(\theta_{k+1,1} - \theta_k) \tag{35}$$

$$\begin{aligned}
M_\theta^{k,2} &= \frac{\partial A(\theta_k)}{\partial \theta_k}x_k + \frac{\partial B_1(\theta_k)}{\partial \theta_k}u + \frac{\partial B_2(\theta_k)}{\partial \theta_k}f(p_k,\beta_k) \\
&+ \frac{1}{2}\frac{\partial A(\theta_k)}{\partial \theta_k}(x_{k+1,1} - x_k) + \frac{1}{2}\left[\frac{\partial^2 A(\theta_k)}{\partial \theta_k^2}x_k + \frac{\partial^2 B_1(\theta_k)}{\partial \theta_k^2}u\right. \\
&\left.+ \frac{\partial^2 B_2(\theta_k)}{\partial \theta_k^2}f(p_k,\beta_k)\right](\theta_{k+1,1} - \theta_k) \\
&+ \frac{1}{2}\frac{\partial B_2(\theta_k)}{\partial \theta_k}\left[\frac{\partial f_k}{\partial p_k}(p_{k+1,1} - p_k) + \frac{\partial f_k}{\partial \beta_k}(\beta_{k+1,1} - \beta_k)\right]
\end{aligned} \tag{36}$$

$$L_x^{k,2} = \begin{bmatrix} B_2(\theta_k) & \frac{1}{2}\frac{\partial B_2(\theta_k)}{\partial \theta_k}(\theta_{k+1,1} - \theta_k) \end{bmatrix} \tag{37}$$

$$N_p^{k,2} = \begin{bmatrix} \frac{\partial f_k}{\partial p_k} + \frac{1}{2}\left(\frac{\partial^2 f_k}{\partial p_k^2}(p_{k+1,1} - p_k) + \frac{\partial^2 f_k}{\partial \beta_k \partial p_k}(\beta_{k+1,1} - \beta_k)\right) \\ \frac{\partial f_k}{\partial p_k} \end{bmatrix} \tag{38}$$

$$N_\beta^{k,2} = \begin{bmatrix} \frac{\partial f_k}{\partial \beta_k} + \frac{1}{2}\left(\frac{\partial^2 f_k}{\partial p_k \partial \beta_k}(p_{k+1,1} - p_k) + \frac{\partial^2 f_k}{\partial \beta_k^2}(\beta_{k+1,1} - \beta_k)\right) \\ \frac{\partial f_k}{\partial \beta_k} \end{bmatrix} \tag{39}$$

$$\begin{aligned}
\eta_x^{k,2} &= \left[A(\theta_k) - M_x^{k,2}\right]x_k + B_1(\theta_k)u + B_2(\theta_k)f(p_k,\beta_k) \\
&- M_\theta^{k,2}\theta_k - M_p^{k,2}p_k - M_\beta^{k,2}\beta_k
\end{aligned} \tag{40}$$

The second step results with the approximations $x_{k+1,2}$, $\theta_{k+1,2}$, and $\beta_{k+1,2}$, which are used in the next iteration of the solution process.

B. Quasi Linearization Based on the Kogan Method

The Kogan method for solution of functional equations was suggested in [23]. It can be obtained from the interpolation function of Eq. (31) by setting $l = 1$, $r_j = 1$, $a_{ij} = 1$, $\gamma_{10} = 0$, and $\gamma_{11} = 1/2$. The method guarantees the third order of convergence [23]. Similar to the method of tangent hyperbolas, the first step of the iteration procedure is an iteration of the classical quasi-linearization technique. At the second step, the Kogan method leads to the following approximation of Eq. (21):

$$\begin{aligned}
\dot{x}_{k+1,2} &= A(\theta_k)x_k + B_1(\theta_k)u + B_2 f(p_k,\beta_k) + A(\tilde{\theta})(x_{k+1,2} - x_k) \\
&+ \left.\frac{\partial A(\theta)}{\partial \theta}\right|_{\theta=\tilde{\theta}} \cdot x_k(\theta_{k+1,2} - \theta_k) + \left.\frac{\partial B_1(\theta)}{\partial \theta}\right|_{\theta=\tilde{\theta}} \cdot u(\theta_{k+1,2} - \theta_k) \\
&+ \left.\frac{\partial B_2(\theta)}{\partial \theta}\right|_{\theta=\tilde{\theta}} \cdot f(\tilde{p},\tilde{\beta})(\theta_{k+1,2} - \theta_k) \\
&+ B_2 \left.\frac{\partial f(p,\beta)}{\partial p}\right|_{p=\tilde{p},\beta=\tilde{\beta}} \cdot (p_{k+1,2} - p_k) \\
&+ B_2 \left.\frac{\partial f(p,\beta)}{\partial \beta}\right|_{p=\tilde{p},\beta=\tilde{\beta}} \cdot (\beta_{k+1,2} - \beta_k)
\end{aligned} \tag{41}$$

where

$$\tilde{\theta} = \theta_k + \tfrac{1}{2}(\theta_{k+1,1} - \theta_k), \qquad \tilde{p} = p_k + \tfrac{1}{2}(p_{k+1,1} - p_k)$$
$$\tilde{\beta} = \beta_k + \tfrac{1}{2}(\beta_{k+1,1} - \beta_k)$$

Therefore, the second-step coefficient matrices of Eq. (24) are defined as

$$M_x^{k,2} = A(\tilde{\theta})$$

$$M_\theta^{k,2} = \left.\frac{\partial A(\theta)}{\partial \theta}\right|_{\theta=\tilde{\theta}} \cdot x_k + \left.\frac{\partial B_1(\theta)}{\partial \theta}\right|_{\theta=\tilde{\theta}} \cdot u + \left.\frac{\partial B_2(\theta)}{\partial \theta}\right|_{\theta=\tilde{\theta}} \cdot f(\tilde{p}, \tilde{\beta}) \tag{42}$$

$$N_p^{k,2} = \left.\frac{\partial f(p,\beta)}{\partial p}\right|_{p=\tilde{p},\beta=\tilde{\beta}}, \qquad N_\beta^{k,2} = \left.\frac{\partial f(p,\beta)}{\partial \beta}\right|_{p=\tilde{p},\beta=\tilde{\beta}} \tag{43}$$

The vector $\eta_x^{k,2}$ is defined according to Eq. (40). The coefficient matrices for Eqs. (25) and (26) are similarly derived.

The Kogan method does not require computation of the second derivatives, which is its obvious advantage when compared with the method of tangent hyperbolas.

VI. Numerical Example

The goal of this numerical study is to demonstrate and validate the suggested identification technique using an aeroelastic model of a generic UAV. The presented model contains nonlinear damping of the control-surface actuator. Nonlinear damping is a typical nonlinearity of aeroelastic structure originating from structural components in sliding contact [24] and leading to limit-cycle oscillations in flight vehicles [25].

A. Test-Case ASE System

The MSC/NASTRAN structural model of the UAV right-hand side is shown in Fig. 2. The weight of the model is 152 kg. The half-span of the wing is 4.0 m and the uniform chord length is 0.55 m. The 4.32-m-long fuselage is modeled by a bar connected to the wing by elastic and rigid structural elements. The model contains 459 grid points and 580 structural elements, leading to 2315 free degrees of freedom. The UAV unsteady aerodynamic model is shown in Fig. 3. The model consists of five aerodynamic panels representing the parts of the wing (three panels), aileron, and elevator/rudder. All of the panels are splined to the structural grid points. More details concerning the UAV models, as well as the results of the stability, dynamic response, and sensitivity analyses, can be found in [26].

State-space modeling and stability analysis was performed using the ASE module of ZAERO [27] software with MSC/NASTRAN [28] aerodynamics. Seventeen generalized aerodynamic force matrices at reduced frequency values between $k = 0.0001$ and 3.6, calculated by MSC/NASTRAN, were exported to ZAERO. The state-space aeroelastic model of the aircraft is constructed using the minimum-state method with physical weighting [19] for aerodynamic approximation. The ASE plant model was obtained by augmentation of the open-loop aeroelastic model with the state-space model of the control-surface actuator (the aerodynamic panel representing the control surface is shadowed in Fig. 3) and with the equation of the pitch-rate sensor located in the centerline of the fuselage near the aircraft center of gravity. The third-order transfer function relating the actuator output δ_c to servo-commanded control-surface deflection u_{ac} (actuator input) was defined as

$$\frac{\delta_c(s)}{u_{ac}(s)} = \frac{6751689.0}{s^3 + 259.97s^2 + 66157.39s + 6751689.0} \tag{44}$$

The resulting state-space ASE plant model includes 28 structural states ξ and $\dot{\xi}$, representing 14 low-frequency symmetric modes (including two rigid-body heave and pitch modes), 7 aerodynamic states x_a, and 3 actuator states δ_c, $\dot{\delta}_c$, and $\ddot{\delta}_c$, leading to the state-space vector

$$x = \left[\xi^T \;\; \dot{\xi}^T \;\; x_a^T \;\; \delta_c^T \;\; \dot{\delta}_c^T \;\; \ddot{\delta}_c^T\right]^T$$

of 38 states. A description of the UAV normal modes is presented in Table 1. Structural damping of $g = 0.01$ is defined for all frequencies. Time-domain stability analysis of the open-loop ASE plant at Mach 0.0 demonstrates a control-surface flutter ($V_F = 39.8$ m/s and $f_F = 37.6$ Hz) of a relatively high frequency between the aileron mode and the third wing-bending mode.

The state-space linear model of the ASE plant constructed for an airspeed of 45 m/s is used for consequent nonlinear modeling. This model defines the matrices A, B_1, C_1, and D_{11} according to Eqs. (13) and (16). The linear model is supplemented by nonlinear damping of the control-surface actuator. The actuator is presented in the finite element model by a spring element located in one of the hinges. The spring interconnects two grid points (one on the wing side and the second on the aileron side) in rotation θ_y. The other rotations and displacements of these points are interconnected rigidly. The nonlinear damping of the actuator is defined by Eq. (11) in the form

$$q = \beta p^3 \tag{45}$$

where $p = (\dot{\theta}_y^{\text{aileron}} - \dot{\theta}_y^{\text{wing}})$ is the relative rotation velocity of the aileron hinge point, q is the nonlinear damping moment, and $\beta = 10.0\ \text{N} \cdot \text{m} \cdot \text{s}^3$ is the constant parameter.

The relative velocity p of the aileron rotation is expressed as

$$p = (\phi_{\text{ah}} - \phi_{\text{wh}})\dot{\xi} + \phi_{\text{ac}}\dot{\delta}_c \tag{46}$$

where ϕ_{ah} and ϕ_{wh} are the θ_y structural modes of the aileron and the

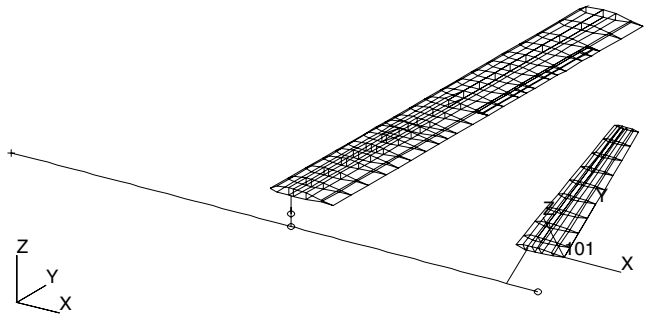

Fig. 2 UAV structural model.

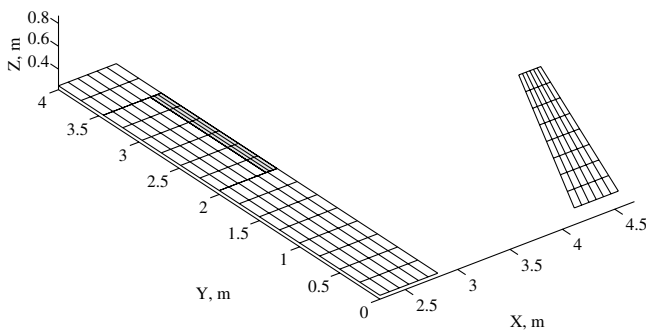

Fig. 3 UAV aerodynamic model.

Table 1 Description of UAV normal modes

Mode no.	Description
1	Heave
2	Pitch
3	First wing bending
4	First wing fore and aft
5	Second wing bending
6	First wing torsion
7	Fuselage bending
8	Aileron bending
9	Third wing bending with aileron rotation
10	Second wing fore and aft with aileron torsion
11	Tail bending
12	Tail torsion
13	Fourth wing bending with aileron torsion
14	Second wing torsion

wing hinge points, and ϕ_{ac} is the control mode of the aileron hinge point.

This definition of the variables p and q enables construction of the matrices B_2, C_2, D_{12}, D_{21}, and D_{22} of Eqs. (8–10) according to Eqs. (18), with $\phi_{nh} = \phi_{ah} - \phi_{wh}$ and $\phi_{nc} = \phi_{ac}$.

B. System Response Analysis

At the first stage of analysis, consider several ASE systems with the linear actuator damping defined by the equation $q = \beta p$ instead of by Eq. (45). The pitch-rate time response of these systems to the actuator step command of 0.1 rad is shown in Fig. 4. The presented results demonstrate that increase of the damping coefficient β stabilizes the system. On the other hand, the rise of the β value increases the oscillations amplitude at the beginning of the response. This amplitude rise is caused by the damping coupling between the control surface and the rest of the aircraft structure, which is represented in the model by the coupling between the structural and control modes. The damping coupling is introduced into the model by the feedback of Eqs. (10) and (11); namely, the element ϕ_{nc} of the matrix C_2 defined by Eqs. (18) is responsible for the modeling of the damping coupling.

The pitch-rate and the aileron-rotation time responses of the nonlinear ASE plant obtained using Simulink software are shown in Figs. 5 and 6 and demonstrate that nonlinear damping leads to stable limit-cycle oscillations (LCO). The nonlinear damping of Eq. (45)

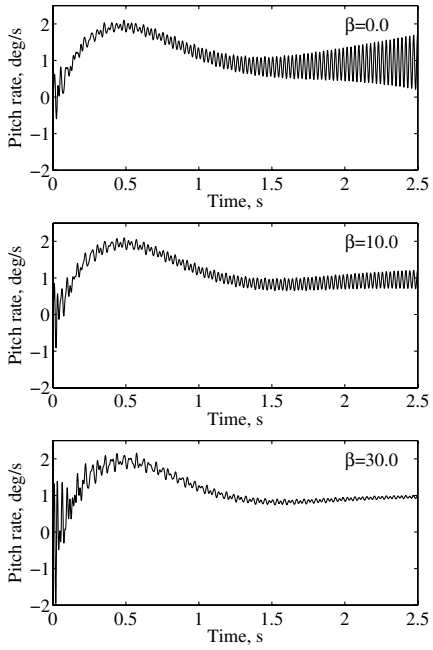

Fig. 4 Pitch-rate response of the linear ASE plant.

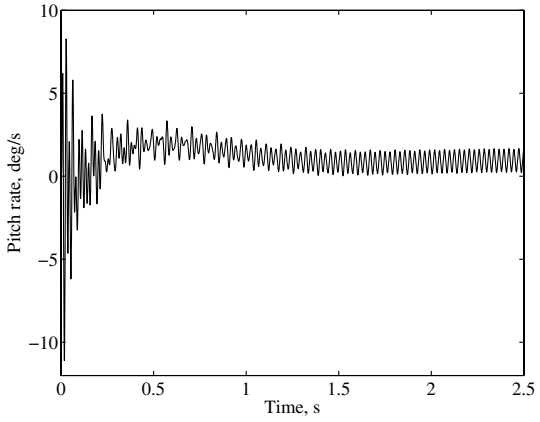

Fig. 5 Pitch-rate response of the nonlinear ASE plant.

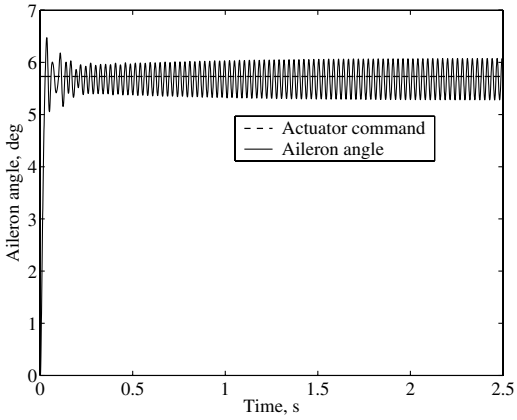

Fig. 6 Aileron-rotation response of the nonlinear ASE plant.

generates a greater damping moment for the large rates of the aileron rotation when compared with the linear damping considered earlier. This leads to greater amplitude of the pitch-rate oscillations at the beginning of the response (when the aileron-rotation rate is very large) when compared with the linear system response of Fig. 4.

C. Identification of the Test-Case System

The goal of the test-case system identification is to apply the developed technique for identification of LFT-interconnected systems and compare the convergence rate and range of the suggested quasi-linearization algorithms. Two parameters of the linear system to be estimated are the (22,8) and (23,9) elements of matrix A of Eq. (8), which are the eighth and ninth diagonal elements of the matrix $-[\bar{M}_{hh}]^{-1}[\bar{K}_{hh}]$. The parameters to be estimated are defined by the generalized structural and aerodynamic stiffnesses of the aileron-bending and the third wing-bending modes (see Table 1) participating in the flutter mechanism that leads to LCO of the nonlinear system. These two parameters are included in the vector θ. The nonlinear damping coefficient β is the third parameter to be estimated. The true values of the estimated parameters are

$$\theta^1_{\text{true}} = -3.4548 \cdot 10^4 \text{ N} \cdot \text{m}, \qquad \theta^2_{\text{true}} = -5.4927 \cdot 10^4 \text{ N} \cdot \text{m}$$

$$\beta_{\text{true}} = 10.0 \text{ N} \cdot \text{m} \cdot \text{s}^3$$

The fragment of the pitch-rate response of Fig. 5 corresponding to the time interval of 0–0.05 s is used as the simulated measured output of the nonlinear system. The measurement data contain 101 evenly distributed discrete measurements. The measured output and the corresponding aileron rotation are shown in Figs. 7 and 8. The initial conditions x_0 being used for simulation of the system output are defined as $x_0 = 0.02 \cdot x(0.01)$, where $x(t)$ is the system state vector corresponding to the actuator step command of 0.1 rad and zero initial conditions. These state initial conditions correspond to a small

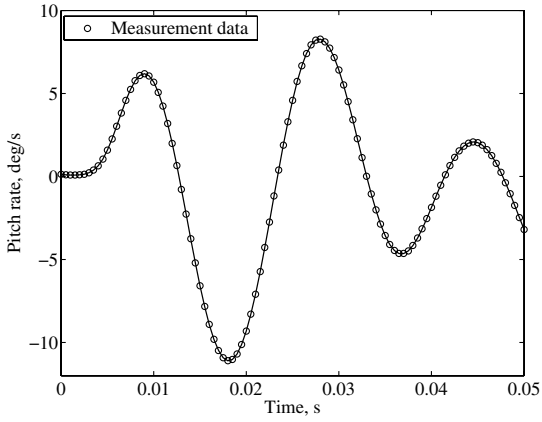

Fig. 7 Measured output of ASE plant.

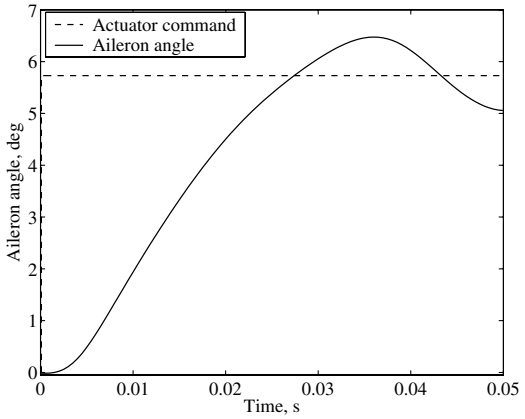

Fig. 8 Aileron rotation corresponding to measured data.

deflection of the aileron (about 0.12 deg). The initial guess θ_0 of the vector of parameters θ is defined as $\theta_0 = 1.5 \cdot \theta_{\text{true}}$. Several initial guesses of the parameter β are used in the estimation process to evaluate the range of convergence of the identification procedures. The initial guess of the state vector $x(t)$ is defined by solution of Eqs. (8–11) for zero initial conditions $x_0(0) = 0$ and the initial guesses of the parameters.

An important stage of system identification is establishing the system identifiability [29]. The system is identifiable if its parameters and initial conditions of the states can be estimated uniquely using input–output measurements. According to Eq. (30), the identifiability requires nonsingularity of the matrix $V_{k+1,j}$ to be inverted. This matrix depends on the product

$$\bar{H}^{k,j}(t)\Omega_{k+1,j}(t_0, t)$$

The matrix $\Omega_{k+1,j}(t_0, t)$ is a sensitivity function of the extended state vector to the extended vector of initial conditions; that is,

$$\Omega_{k+1,j}(t_0, t) = \partial z_k(t)/\partial z_k(t_0)$$

(see [30]). The product

$$\bar{H}^{k,j}\Omega_{k+1}(t_0, t) = \partial y_k(t)/\partial z_k(t_0)$$

is the sensitivity function $Y_z(t_0, t)$ of the vector of measurements to the extended vector of initial conditions. The supremum norm of the components of the sensitivity function $Y_z(t_0, t)$ calculated for the initial guesses $x_0(0)$ and θ_0 (defined earlier) and $\beta_0 = 20$ is presented in Table 2. Description of the aircraft normal modes presented in Table 1 indicates that the greatest sensitivities of the pitch-rate output correspond to the normal modes containing the aileron and tail deformations. High sensitivity of the state ξ_{14} corresponding to the second wing-torsion mode is caused by a large deformation of the wingtip area, which includes the aileron as well.

The heave mode is unobservable for the pitch-rate output, and so the sensitivity of the pitch output to the initial condition for the first state ξ_1 is zero, as shown in Table 2. This leads to singularity of the matrix V_{k+1}. To avoid the singularity, the heave initial condition can be set to zero and eliminated from the process of estimation, because it does not influence the system's measured output. Nevertheless, the matrix V_{k+1} remains close to singular because of the other relatively small components of the function $Y_z(t_0, t)$ (the reciprocal condition number for the matrix V_{k+1} is of the order of magnitude of 10^{-26}, and the floating point relative accuracy of computation is 10^{-16}).

Table 2 Supremum norm of the components of the sensitivity function $Y_z(0, t)$

No.	State	State no.	$\|Y_z\|_\infty$	No.	State	State no.	$\|Y_z\|_\infty$
1	ξ_{14}	14	3.64e + 01	22	$\dot{\xi}_2$	16	7.03e − 02
2	ξ_{12}	12	2.04e + 01	23	$\dot{\xi}_2$	2	6.86e − 02
3	ξ_{13}	13	1.31e + 01	24	$\dot{\xi}_{12}$	26	6.38e − 02
4	ξ_{10}	10	8.78e + 00	25	$\dot{\xi}_{13}$	27	3.65e − 02
5	ξ_9	9	8.31e + 00	26	$\dot{\xi}_3$	3	3.23e − 02
6	ξ_8	8	7.42e + 00	27	$\dot{\xi}_{10}$	24	3.14e − 02
7	x_{a5}	33	5.74e + 00	28	$\dot{\xi}_9$	23	2.74e − 02
8	x_{a4}	32	5.38e + 00	29	$\dot{\xi}_6$	20	2.46e − 02
9	ξ_{11}	11	3.86e + 00	30	$\dot{\xi}_8$	22	2.33e − 02
10	ξ_7	7	2.64e + 00	31	$\dot{\delta}$	37	2.32e − 02
11	ξ_6	6	2.30e + 00	32	$\dot{\xi}_7$	21	1.96e − 02
12	δ	36	1.99e + 00	33	θ^1	40	1.47e − 02
13	x_{a2}	30	1.30e + 00	34	$\dot{\xi}_{11}$	25	1.26e − 02
14	x_{a3}	31	1.18e + 00	35	$\dot{\xi}_5$	19	7.60e − 03
15	x_{a7}	35	6.85e − 01	36	θ^2	41	3.85e − 03
16	ξ_5	5	6.52e − 01	37	$\dot{\xi}_3$	17	2.79e − 03
17	x_{a1}	29	5.61e − 01	38	$\dot{\xi}_1$	15	1.56e − 03
18	x_{a6}	34	5.52e − 01	39	$\dot{\xi}_4$	18	7.76e − 04
19	$\dot{\xi}_{14}$	28	1.09e − 01	40	$\ddot{\delta}$	38	6.65e − 05
20	β	39	9.20e − 02	41	ξ_1	1	0.00e + 00
21	ξ_4	4	7.58e − 02				

To obtain a numerically stable identification process, more components of the vector x_0 should be eliminated from the estimation procedure. To evaluate the influence of this elimination on the accuracy of the estimates, the identification procedure was performed for three sets of estimated initial conditions. The first set is empty (no initial conditions were estimated). The second set includes initial conditions of the six states $\xi_{14}, \xi_{12}, \xi_{13}, \xi_{10}, \xi_9$, and ξ_8, with the greatest norm $\|Y_z\|_\infty$ (see Table 2). The third set contains the initial conditions of the second set, without ξ_{12} and ξ_{13}. The estimation accuracy was defined by the mean squared value J/N of the error between the outputs of the plant and the model [see Eq. (5)]. The mean squared value of the plant output is 7.4838×10^{-3} s^{-2}. Convergence of the iteration process was established according to the requirement

$$\|e_{k+1}\|_\infty \le 10^{-3}$$

where the components e^i_{k+1} of the vector e_{k+1} were defined as

$$e^i_{k+1} = \left(\alpha^i_{k+1} - \alpha^i_k\right) \Big/ \alpha^i_k$$

with $\alpha_k = [\,\theta^T_k \quad \beta^T_k\,]^T$. Estimation results for the three sets of estimated initial conditions and the reciprocal of the condition number, R_{cond}, for the matrix V_1 are presented in Table 3 (the true values of the parameters are presented for comparison). The presented results demonstrate that even for the first case, the estimates are acceptable: the mean squared error is three orders of magnitude lower than the mean squared plant output, in spite of the rather inaccurate β estimate. The discrepancy between the estimates and the true values of the parameters is caused by the difference between the true values of the nonestimated initial conditions and the zero values being used in the estimation process. Estimation of the

Table 3 Estimation results

Set no.	θ^1, N · m	θ^2, N · m	β, N · m · s^3	J/N, s^{-2}	R_{cond}
1	-3.4467×10^4	-5.5484×10^4	9.3846	1.4295×10^{-6}	4.9758×10^{-3}
2	-3.4437×10^4	-5.6075×10^4	9.9442	2.0426×10^{-7}	1.5652×10^{-10}
3	-3.4668×10^4	-5.4130×10^4	9.9451	2.3535×10^{-7}	6.3137×10^{-10}
True	-3.4548×10^4	-5.4927×10^4	10.0	0	——

Table 4 Number of steps required for convergence of estimation procedure

	Initial guess of β							
Method	5	20	25	30	35	40	45	50
QL2	D[a]	10	9	17[b]	15[b]	18[b]	D[a]	D[a]
TH	D[a]	9	9	6	9	16[b]	12[b]	10[b]
Kogan	D[a]	6	7	7	8	8	18[b]	14[b]

[a]Divergence of iteration process.
[b]Convergence to solution $\theta = [-3.768 \times 10^4 \quad -4.586 \times 10^4]$, $\beta = 20.75$.

initial conditions considerably improves the estimation accuracy, but reduces the R_{cond} value. Nevertheless, the obtained R_{cond} values are six orders of magnitude greater than the floating point computations accuracy, which is enough for numerically stable computations. The third case is selected for consequent analysis because it provides greater R_{cond} than, and the same accuracy as, the second case.

Comparing the computational effectiveness of the methods under consideration, one should take into account that one iteration of a third-order algorithm contains two steps, and so it is twice as costly as one iteration of the Bellman–Kalaba method. Hence, the number of steps (not iterations) required for convergence of the algorithm should be considered for comparison of computational effectiveness of the methods. The number of steps for various initial guesses of the parameter β is presented in Table 4. One can see that all of the methods diverge for $\beta_0 = 5$. The region of convergence contains the initial guesses exceeding the true value of β. The second-order quasi-linearization method demonstrates convergence to the true parameter values for $\beta_0 \leq 25$: the method of tangent hyperbolas converges for $\beta_0 \leq 35$, and the Kogan method converges for $\beta_0 \leq 40$. The further rise of the β_0 values leads to convergence to the solution

$$\theta = [-3.768 \times 10^4 \quad -4.586 \times 10^4]$$

and $\beta = 20.75$. The mean squared value of the error $(y - y^M)$ for this solution is equal to 3.0838×10^{-6}, which is three orders of magnitude smaller than the mean squared value of the plant output, but one order of magnitude greater than the J/N value for the correct solution presented in Table 3. The second-order quasi-linearization algorithm diverges for the β initial guesses of 45 and 50. The results of Table 3 demonstrate the advantages of the third-order methods in computational efficiency and in size of the range of convergence. Comparison of the convergence rate and range of the third-order algorithms shows that the Kogan method is more effective than the method of tangent hyperbolas. As pointed out earlier, an additional advantage of the Kogan method is that it does not require computation of the second-order derivatives.

Iteration history of the estimation for the case of convergence of all of the methods to the correct solution is presented in Fig. 9. The convergence of the Bellman–Kalaba and tangent-hyperbola methods to the wrong solution is shown in Fig. 10.

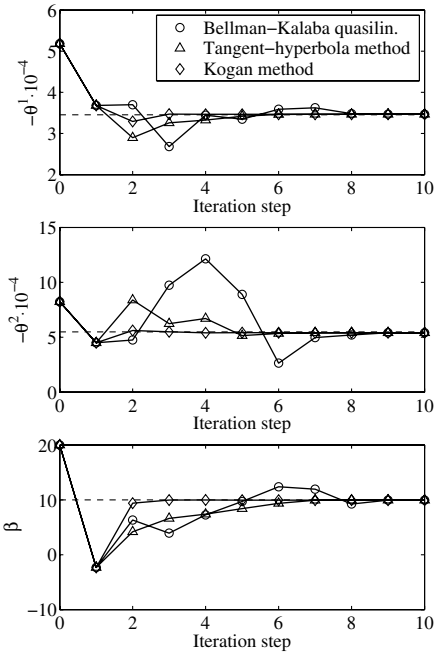

Fig. 9 Convergence of iterative processes for $\beta_0 = 20$.

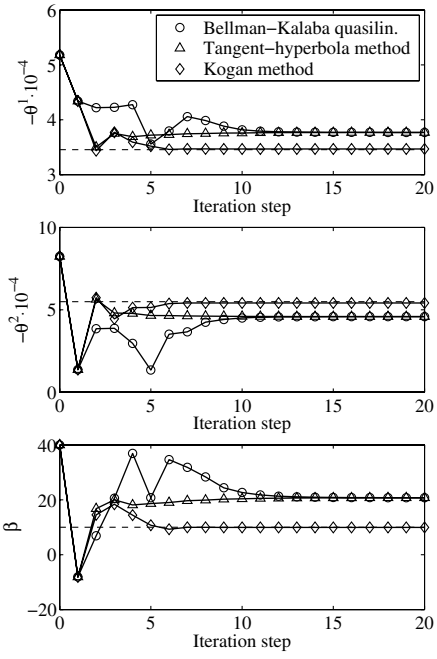

Fig. 10 Convergence of iterative processes for $\beta_0 = 40$.

VII. Conclusions

The quasi-linearization technique for parametric identification is extended in this work to enable parameter estimation of LFT-modeled nonlinear dynamic systems. High-order quasi-linearization procedures for identification of these systems are developed. The systems under consideration are modeled by LFT interconnection containing a linear dynamic system in the feedforward pass and a static nonlinear element in the feedback loop. The proposed approach for synthesis of the high-order quasi-linearization procedures enables construction of a variety of algorithms. It is applied for synthesis of two third-order-of-convergence procedures based on the methods of tangent hyperbolas and Kogan for solution of functional equations. These new algorithms are compared with the second-order-of-convergence classical Bellman–Kalaba quasi-linearization procedure.

The final section of the paper demonstrates application of the developed technique using a realistic test-case UAV model with nonlinear damping of the control-surface actuator. It is shown that the estimation of parameters and state initial conditions of ASE systems may lead to a singular problem because of relatively small or zero sensitivities of the measurements to some initial conditions. These initial conditions were set equal to their initial guesses and eliminated from the estimation process with minor effect on the estimates accuracy. Simulation results demonstrate that the range and rate of convergence of the suggested third-order methods are greater in comparison with the second-order quasi-linearization technique. According to this criterion, the Kogan method is more effective than the method of tangent hyperbolas. An additional advantage of the Kogan method is its computational simplicity when compared with the tangent-hyperbola method.

Appendix A: Matrix Coefficients of the Model

The matrix coefficients of Eqs. (24–26) for $j = 1$ are defined as follows:

$$
\begin{aligned}
M_x^{k,1} &= A(\theta_k)\\
M_\theta^{k,1} &= \frac{\partial A(\theta_k)}{\partial \theta_k} x_k + \frac{\partial B_1(\theta_k)}{\partial \theta_k} u + \frac{\partial B_2(\theta_k)}{\partial \theta_k} f(p_k, \beta_k)\\
L_x^{k,1} &= B_2(\theta_k)
\end{aligned} \tag{A1}
$$

$$
\begin{aligned}
H_x^{k,1} &= C_1(\theta_k)\\
H_\theta^{k,1} &= \frac{\partial C_1(\theta_k)}{\partial \theta_k} x_k + \frac{\partial D_{11}(\theta_k)}{\partial \theta_k} u + \frac{\partial D_{12}(\theta_k)}{\partial \theta_k} f(p_k, \beta_k)\\
L_y^{k,1} &= D_{12}(\theta_k)
\end{aligned} \tag{A2}
$$

$$
\begin{aligned}
G_x^{k,1} &= C_2(\theta_k)\\
G_\theta^{k,1} &= \frac{\partial C_2(\theta_k)}{\partial \theta_k} x_k + \frac{\partial D_{21}(\theta_k)}{\partial \theta_k} u + \frac{\partial D_{22}(\theta_k)}{\partial \theta_k} f(p_k, \beta_k)\\
L_p^{k,1} &= D_{22}(\theta_k)
\end{aligned} \tag{A3}
$$

$$
N_p^{k,1} = \frac{\partial f_k}{\partial p_k}, \qquad N_\beta^{k,1} = \frac{\partial f_k}{\partial \beta_k} \tag{A4}
$$

$$
\begin{aligned}
\eta_x^{k,1} = {} & B_1(\theta_k)u + B_2(\theta_k) f(p_k, \beta_k) - M_\theta^{k,1}\theta_k - L_x^{k,1} N_p^{k,1} p_k\\
& - L_x^{k,1} N_\beta^{k,1} \beta_k
\end{aligned} \tag{A5}
$$

$$
\begin{aligned}
\eta_y^{k,1} = {} & D_{11}(\theta_k)u + D_{12}(\theta_k) f(p_k, \beta_k) - H_\theta^{k,1}\theta_k - L_y^{k,1} N_p^{k,1} p_k\\
& - L_y^{k,1} N_\beta^{k,1} \beta_k
\end{aligned} \tag{A6}
$$

$$
\begin{aligned}
\eta_p^{k,1} = {} & D_{21}(\theta_k)u + D_{22}(\theta_k) f(p_k, \beta_k) - G_\theta^{k,1}\theta_k - L_p^{k,1} N_p^{k,1} p_k\\
& - L_p^{k,1} N_\beta^{k,1} \beta_k
\end{aligned} \tag{A7}
$$

The elements of the products containing the derivatives of the system matrices with respect to vector θ [e.g., $P = (\partial B/\partial\theta)u\theta$] are calculated as

$$
P_i = \sum_{l=1}^{d} \left(\sum_{j=1}^{m} \frac{\partial B_{ij}}{\partial \theta_l} u_j \right) \theta_l
$$

where $i = 1, \ldots, n$; n and m are the dimensions of the matrix B; and d is the number of components of the vector θ. This simplified notation of the products containing multidimensional matrices is used in the entire paper.

Appendix B: Matrix Coefficients of the Linearized Model

The matrix coefficients of Eqs. (19) and (20) are defined as follows:

$$
\begin{aligned}
\bar{M}_x^{k,j} &= \mathcal{F}_\ell\left(\begin{bmatrix} M_x^{k,j} & L_x^{k,j} \\ G_x^{k,j} & L_p^{k,j} \end{bmatrix}, N_p^{k,j} \right)\\
\bar{M}_\theta^{k,j} &= \mathcal{F}_\ell\left(\begin{bmatrix} M_\theta^{k,j} & L_x^{k,j} \\ G_\theta^{k,j} & L_p^{k,j} \end{bmatrix}, N_p^{k,j} \right)\\
\bar{M}_\beta^{k,j} &= \mathcal{F}_\ell\left(\begin{bmatrix} L_x^{k,j} & L_x^{k,j} \\ L_p^{k,j} & L_p^{k,j} \end{bmatrix}, N_p^{k,j} \right) N_\beta^{k,j}\\
\bar{\eta}_x^{k,j} &= \mathcal{F}_\ell\left(\begin{bmatrix} \eta_x^{k,j} & L_x^{k,j} \\ \eta_p^{k,j} & L_p^{k,j} \end{bmatrix}, N_p^{k,j} \right)
\end{aligned}
$$

$$
\begin{aligned}
\bar{H}_x^{k,j} &= \mathcal{F}_\ell\left(\begin{bmatrix} H_x^{k,j} & L_y^{k,j} \\ G_x^{k,j} & L_p^{k,j} \end{bmatrix}, N_p^{k,j} \right)\\
\bar{H}_\theta^{k,j} &= \mathcal{F}_\ell\left(\begin{bmatrix} H_\theta^{k,j} & L_y^{k,j} \\ G_\theta^{k,j} & L_p^{k,j} \end{bmatrix}, N_p^{k,j} \right)\\
\bar{H}_\beta^{k,j} &= \mathcal{F}_\ell\left(\begin{bmatrix} L_y^{k,j} & L_y^{k,j} \\ L_p^{k,j} & L_p^{k,j} \end{bmatrix}, N_p^{k,j} \right) N_\beta^{k,j}\\
\bar{\eta}_y^{k,j} &= \mathcal{F}_\ell\left(\begin{bmatrix} \eta_y^{k,j} & L_y^{k,j} \\ \eta_p^{k,j} & L_p^{k,j} \end{bmatrix}, N_p^{k,j} \right)
\end{aligned}
$$

where $\mathcal{F}_\ell(\cdot,\cdot)$ is the notation of LFT.

Acknowledgments

The work presented in this paper was supported by a joint grant from the Israeli Ministry of Immigrant Absorption and the Council for Higher Education.

References

[1] Mehra, R. K., and Prasanth, R. K., "Time-Domain System Identification Methods for Aeromechanical and Aircraft Structural Modeling," *Journal of Aircraft*, Vol. 41, No. 4, 2004, pp. 721–729.

[2] Wang, K. C., and Iliff, K. W., "Retrospective and Recent Examples of Aircraft Parameter Identification at NASA Dryden Flight Research Center," *Journal of Aircraft,* Vol. 41, No. 4, 2004, pp. 752–764.

[3] Wolodkin, G., Rangan, S., and Poolla, K., "An LFT Approach to Parameter Estimation," *Proceedings of the 1997 American Control Conference* [CD-ROM], American Automatic Control Council, Evanston, IL, 1997.

[4] Lind, R., Prazenica, R., and Brenner, M., "Estimating Nonlinearity Using Volterra Kernels in Feedback with Linear Models," Proceedings of the 44th AIAA/ASME/ ASCE/AHS/ASC Structures, Structural Dynamics, and Materials Conference, Norfolk, VA, AIAA Paper 2003-1406, Apr. 2003.

[5] Baldelli, D. H., Chen, P., Liu, D., Lind, R., and Brenner, M., "Nonlinear Aeroelastic Modeling by Block-Oriented Identification," Proceedings of the 45th AIAA/ASME/ASCE/AHS/ASC Structures, Structural Dynamics, and Materials Conference, Palm Springs, CA, AIAA Paper 2004-1938, Apr. 2004.

[6] Bellman, R. E., and Kalaba, R. E., *Quasilinearization and Nonlinear Boundary-Value Problems*, Elsevier, New York, 1965.

[7] Sage, A., and Melsa, J., *System Identification*, Academic Press, New York, 1971, pp. 152–180.

[8] Roberts, S. M., and Shipman, J. S., *Two-Point Boundary Value Problems: Shooting Methods*, Elsevier, New York, 1972, pp. 232–245.

[9] Nechepurenko, M. I., "On Chebyshev Method for Functional Equations," *Uspekhi Matematicheskikh Nauk*, Vol. 9, No. 2, 1954, pp. 162–170 (in Russian).

[10] Moore, R. H., "Newton's Method and Variations," *Nonlinear Integral Equations*, edited by P. Anselone, Univ. of Wisconsin Press, Madison, WI, 1964, pp. 65–98.

[11] Mertvetsova, M. A., "Analogue of the Process of Tangent Hyperbolas for General Functional Equations," *Doklady Akademii nauk SSSR*, Vol. 88, No. 4, 1953, pp. 611–614 (in Russian).

[12] Moulin, B., "Parametric Identification of Nonlinear Systems Based on Iteration Methods for Solution of Functional Equations," Ph.D. Thesis, Omsk Inst. of Railroad Engineering, Omsk, Russia, 1986 (in Russian).

[13] Hamel, P. G., and Jategaonkar, R. V., "Evolution of Flight Vehicle System Identification," *Journal of Aircraft*, Vol. 33, No. 1, 1996, pp. 9–28.

[14] Larson, D. B., and Fleck, J. T., "Identification of Parameters by the Method of Quasilinearization," Cornell Aeronautical Lab., Rept. 164, Buffalo, NY, 1968.

[15] Taylor, L. W., Jr., and Iliff, K. W., "A Modified Newton–Raphson Method for Determining Stability Derivatives from Flight Data," *Computing Methods in Optimization Problems*, Academic Press, New York, 1969, pp. 353–364.

[16] Taylor, L. W., Jr., and Iliff, K. W., "System Identification Using a Modified Newton–Raphson Method—A Fortran Program," NASA TN D-6734, May 1972.

[17] Eykhoff, P., *System Identification*, Wiley, London, 1974, pp. 455–457.

[18] Idan, M., Karpel, M., and Moulin, B., "Aeroservoelastic Interaction Between Aircraft Structural and Control Design Schemes," *Journal of Guidance, Control, and Dynamics*, Vol. 22, No. 4, 1999, pp. 513–519.

[19] Karpel, M., "Time-Domain Aeroservoelastic Modeling Using Weighted Unsteady Aerodynamic Forces," *Journal of Guidance, Control, and Dynamics*, Vol. 13, No. 1, 1990, pp. 30–37.
[20] Karpel, M., "Multidisciplinary Optimization of Aeroservoelastic Systems Using Reduced-Size Models," *Journal of Aircraft*, Vol. 29, No. 5, 1992, pp. 939–946.
[21] Moulin, B., "Modeling of Aeroservoelastic Systems with Structural and Aerodynamic Variations," *AIAA Journal*, Vol. 43, No. 12, 2005, pp. 2503–2513.
[22] Traub, J. F., *Iterative Methods for the Solution of Equations*, Prentice–Hall, Englewood Cliffs, NJ, 1964, pp. 161–163.
[23] Kogan, T. I., "An Iteration Process for Functional Equations," *Siberian mathematical Journal*, Vol. 8, No. 4, 1967, pp. 727–729.
[24] Dowell, E. H., and Tang, D., "Nonlinear Aeroelasticity and Unsteady Aerodynamics," *AIAA Journal*, Vol. 40, No. 9, 1990, pp. 1697–1707.
[25] Mignolet, M. P., Liu, D. D., and Chen, P. C., "On the Nonlinear Structural Damping Mechanism of the Wing/Store Limit Cycle Oscillation," AIAA Paper 99-1459, 1999.
[26] Moulin, B., Feldgun, V., and Karpel, M., "Application of the State-Space Equation of the Integrated System in Stability and Response Analyses Including Sensitivity Evaluation," Faculty of Aerospace Engineering, Technion—Israel Inst. of Technology, TR 899, Haifa, Israel, July 2002.
[27] Anon., *ZAERO Version 7.3. Theoretical Manual*,ZONA Technology Inc., Scottsdale, AZ, Mar. 2005.
[28] Rodden, W. P., *Handbook of Aeroelastic Analysis: MSC/NASTRAN Version 65*, Vol. 1, MacNeal–Schwendler Corp., Los Angeles, 1987.
[29] Kalaba, R. E., and Spingarn, K., "Control, Identification, and Input Optimization," Plenum, New York, 1982, pp. 299–301.
[30] Rosenwasser, E., and Yusupov, R., "Sensitivity of Automatic Control Systems," CRC Press, Boca Raton, FL, 2000, pp. 23–33.